Mucosal Immunology 17 (2024) 1326–1336

Contents lists available at ScienceDirect

Mucosal Immunology

journal homepage: www.elsevier.com/mi

Article

Dysregulated NOX1-NOS2 activity as hallmark of ileitis in mice

Julie Drieu La Rochelle [a,5], Josie Ward [a,1,5], Emily Stenke [a,2], Yuting Yin [a,3], Misaki Matsumoto [b,4], Richard Jennings [a], Gabriella Aviello [c], Ulla G. Knaus [a,*]

[a] UCD Conway Institute, School of Medicine, University College Dublin, Dublin, Ireland
[b] Department of Pharmacology, Kyoto Prefectural University of Medicine, Kyoto, Japan
[c] Department of Pharmacy, University of Naples Federico II, Naples, Italy

A B S T R A C T

Inflammation of the ileum, or ileitis, is commonly caused by Crohn's disease (CD) but can also accompany ulcerative colitis (backwash ileitis), infections or drug-related damage. Oxidative tissue injury triggered by reactive oxygen species (ROS) is considered part of the ileitis etiology. However, not only elevated ROS but also permanently decreased ROS are associated with inflammatory bowel disease (IBD). While very early onset IBD (VEO-IBD) is associated with a spectrum of *NOX1* variants, how NOX1 inactivation contributes to disease development remains ill-defined. Besides propagating signaling responses, NOX1 provides superoxide for peroxynitrite formation in the epithelial barrier. Here we report that NOX4, an H_2O_2-generating NADPH oxidase with documented tissue protective effects in the intestine and other tissues, limits the generation of ileal peroxynitrite by NOX1/NOS2. Deletion of NOX4 leads to persistent peroxynitrite excess, hyperpermeability, villus blunting, muscular hypertrophy, chemokine/cytokine upregulation and dysbiosis. Conversely, SAMP1/YitFc mice, a CD-like ileitis model, showed age-dependent NOX1/NOS2 downregulation preventing ileal peroxynitrite formation in homeostasis and LPS-induced acute inflammation. Deficiency in NOX1 correlated with the upregulation of antimicrobial peptides, suggesting that ileal peroxynitrite acts as chemical barrier and microbiota modifier in the ileum.

Introduction

Reactive oxygen species (ROS) are associated with maintaining homeostasis, signaling responses and host defense, but also with inflammation and tissue destruction. This dichotomy stems from ROS chemistry, kinetics, and the extent, duration, and location of ROS generation. In the gastrointestinal tract these oxygen-derived species regulate mucus layer maintenance and bi-directional communication with the commensal microbiota, both key to epithelial barrier integrity. Further, certain oxygen/nitrogen species are essential host defense mechanisms ranging from repellant and antivirulence effects to pathogen killing[1–6]. These beneficial attributes are reflected in the association of pathogenic variants in ROS-generating NADPH oxidases (e.g., loss-of-function *NOX1/DUOX2* variants) with very early onset inflammatory bowel disease (VEO-IBD)[7–9], and in the 40–50 % of patients with chronic granulomatous disease (CGD) who develop IBD as part of their primary immunodeficiency due to compromised NOX2 complex function[10,11]. On the other hand, continuous production of highly reactive hydroxyl radicals, hypochlorous acid (HOCl), peroxynitrite ($ONOO^-$) and other reactive oxygen/nitrogen metabolites drives inflammatory processes connected to intestinal tissue injury[12,13]. Chronic inflammation may also fuel the survival of pathogens that can upregulate detoxification mechanisms and derive a competitive advantage from oxidized gut microbiota-derived metabolites[14,15].

Our current understanding supports the idea of context-dependent positive and negative consequences of NOX1, NOX2, and DUOX2 activity in the gastrointestinal tract. In contrast, recent data suggest that NOX4 may function primarily as a gut mucosa-protective oxidase. Endogenous expression of NOX4, a constitutively active oxidase, ameliorated acute chemical and bacterial colitis in mice[2,16,17]. In other organs, NOX4-derived H_2O_2 prevented hyperinflammation and sustained a beneficial oxidative tone in vascular remodeling, atherosclerosis and cell differentiation[18–20]. In several cell types including cardiomyocytes, cancer-associated fibroblasts, and hepatocytes this effect has been linked to NOX4-mediated pro-survival signaling via KEAP2/NRF2, a master regulator of the antioxidant response[21–23]. In a

* Corresponding author at: Conway Institute, University College Dublin, Belfield, Dublin 4, Ireland.
E-mail address: ulla.knaus@ucd.ie (U.G. Knaus).
[1] Present address: Charles Institute of Dermatology, School of Medicine, University College Dublin, Dublin, Ireland.
[2] Present address: National Centre for Pediatric Gastroenterology, Children's Health Ireland at Crumlin, Dublin, Ireland.
[3] Present address: Research Development Office, Maynooth University, Maynooth, Ireland.
[4] Present address: Department of Clinical Pharmacology and Pharmacotherapy, Wakayama Medical University, Wakayama, Japan.
[5] Equal contribution.

https://doi.org/10.1016/j.mucimm.2024.08.012
Received 25 April 2024; Accepted 31 August 2024
Available online 7 September 2024
1933-0219/© 2024 The Author(s). Published by Elsevier Inc. on behalf of Society for Mucosal Immunology. This is an open access article under the CC BY license (http://creativecommons.org/licenses/by/4.0/).

colitis-associated carcinoma model *Nox4* deletion caused genomic instability due to altered oxidation and phosphorylation of the protein kinase AKT that increased nuclear translocation of the phosphatase PP2A and γH2AX dephosphorylation, thereby weakening DNA damage recognition and repair[24].

The possibility that NOX4 might be a homeostatic rheostat for differentiation programs and a promoter of the cell/tissue redox equilibrium in the highly regenerative intestine, led us to perform detailed studies of NOX4 deficient mice at steady state. Here we report that *Nox4* deletion in mice results in spontaneous age-dependent damage to the ileal epithelium in environmentally controlled conditions. Ileal NOX4 is required to dampen peroxynitrite formation generated by combined NOX1-NOS2 activity. Sustaining moderate peroxynitrite production in a regulated manner is likely a prerequisite for maintaining a host-microbe equilibrium in the ileum, as the NOX1-NOS2 axis is also dysfunctional in the Crohn's disease (CD)-like SAMP1/YitFc ileitis model.

Results

Loss of ileal epithelial integrity in NOX4-deficient mice

The protective role of NOX4 in murine models of acute bacterial and chemical colitis prompted closer evaluation of the gastrointestinal tract of *Nox4*$^{-/-}$ mice at homeostasis. The gastrointestinal transit time was accelerated in *Nox4*$^{-/-}$ mice and the intestinal barrier showed increased permeability (Fig. 1A and B). Histology indicated age-dependent alterations in the small intestine with blunted and irregular villi, immune cell infiltration, and muscularis mucosae hyperplasia *in* older mice (16 weeks) (Fig. 1C). This phenotype was confirmed with SEM images where cell debris was frequently visible on or surrounding the tips of blunted villi (Fig. 1D). The apparent epithelial damage in the ileum triggered evaluation of the chemical microenvironment in this gut region. We analyzed the *in vivo* generation of reactive oxygen/nitrogen species (RONS) in wildtype and *Nox4*$^{-/-}$ mice by injecting 16-week-old mice with the luminol derivative L-012 to follow RONS generation in real time in living mice[2,25]. In whole body kinetics the total photon flux

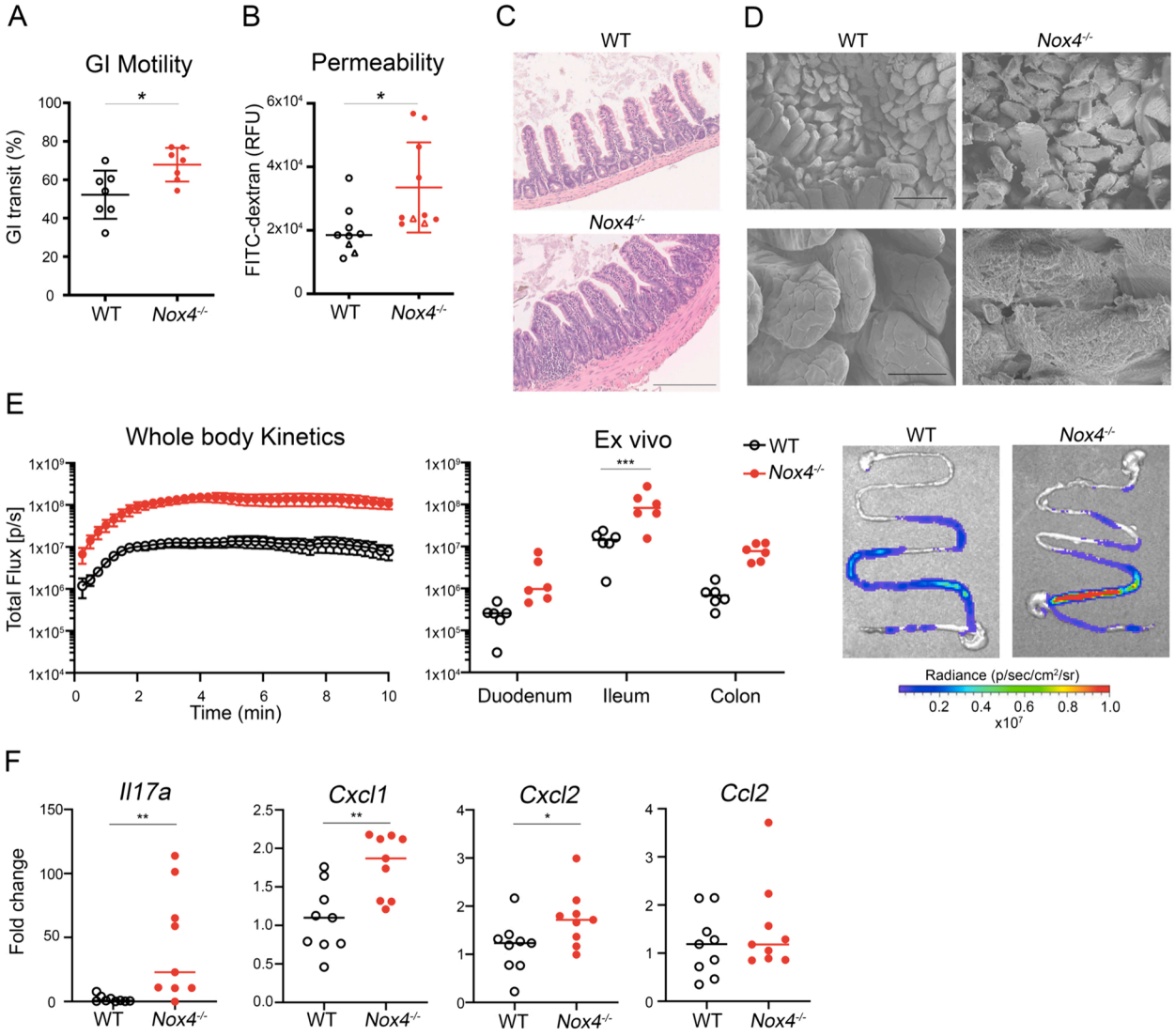

Fig. 1. Increased ileal ROS generation in *Nox4*$^{-/-}$ mice causes epithelial damage. (A) Intestinal motility was determined by oral charcoal administration (n = 7/group). (B) Intestinal permeability was analyzed using oral FITC-dextran (n = 9–10/group, circles = 6-wk-old, triangles = 16 wk-old). (C) H&E-stained ileal sections of WT and *Nox4*$^{-/-}$ mice, scale bar 200 μm. (D) SEM images of ileal sections of WT *and Nox4*$^{-/-}$ mice, scale bar 200 μm (top), 50 μm (bottom). (E) WT and *Nox4*$^{-/-}$ mice were injected with L-012 directly before IVIS imaging, followed by *ex vivo* imaging of intestines. Abdominal kinetic curves, regional analysis of intestinal flux, and representative images of excised intestines (n = 6/group). (F) Ileal expression of indicated genes in WT and *Nox4*$^{-/-}$ mice (n = 9/group). Two-way ANOVA with multiple comparisons test performed on normalized data (E), *t*-test (A, B and F) (*Cxcl1*, *Cxcl2*), or Mann-Whitney test on F (*Il17a*, *Ccl2*).

was markedly increased in *Nox4*$^{-/-}$ mice *in vivo* (Fig. 1E). A significantly increased flux was observed in the terminal ileum *ex vivo*, the area of the most pronounced epithelial damage in histology and SEM (Fig. 1E). Amplification of the ileal L-012 signal was age-dependent and more consistently recorded in male *Nox4*$^{-/-}$ mice at 16-weeks and older, suggesting that the enhanced RONS phenotype is either slower to develop or less consistent in female *Nox4*$^{-/-}$ mice (Fig. S1A). Anti-Mucin2 immunofluorescence in ileal tissues derived from wildtype

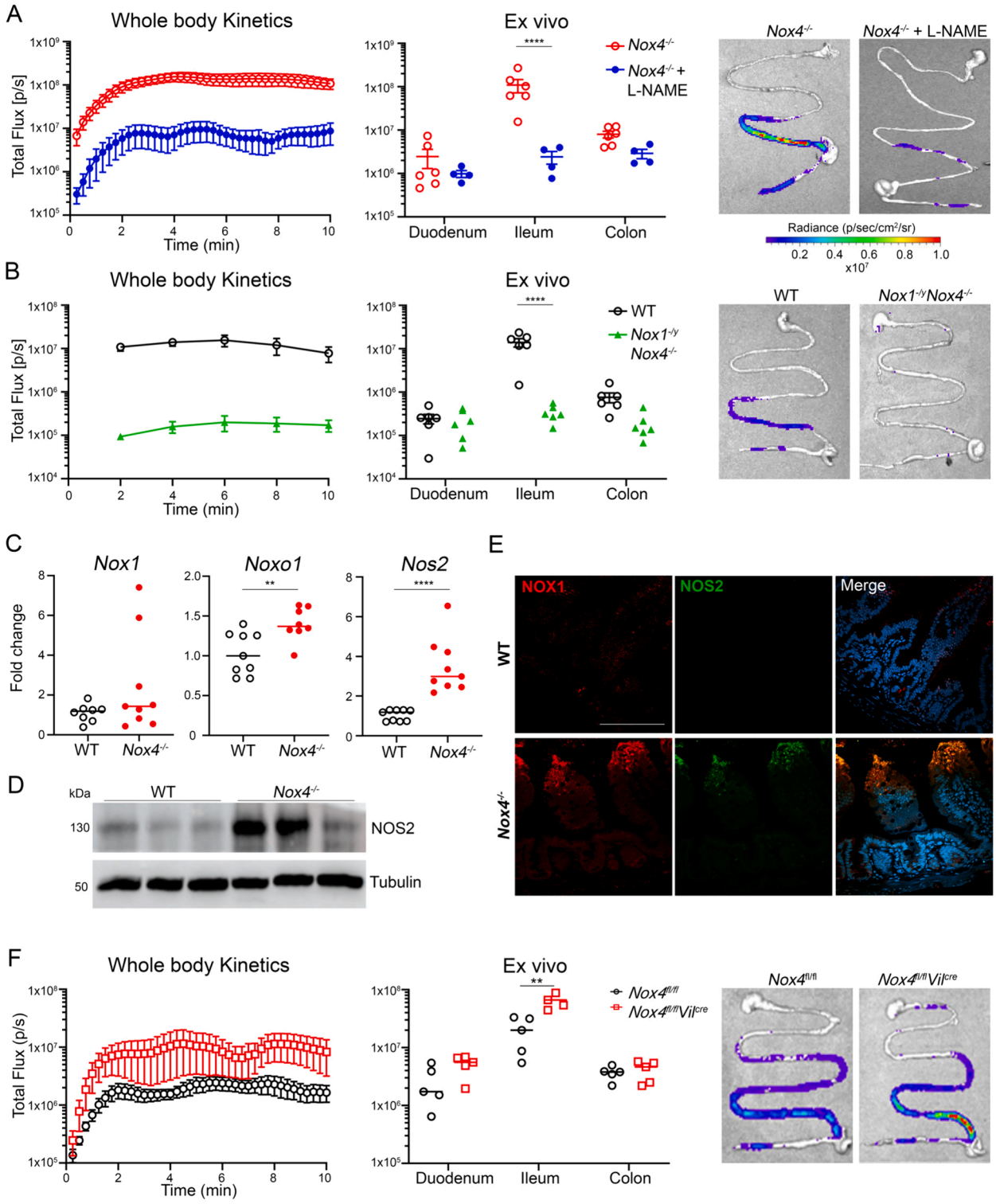

Fig. 2. Ileal peroxynitrite generation in *Nox4*$^{-/-}$ mice is NOX1 and NOS2 dependent. (A) *Nox4*$^{-/-}$ mice were injected with L-NAME or vehicle 6 h before L-012 injection and IVIS imaging. Kinetic curves, ex vivo analysis, and representative images of excised intestines are shown (n = 4–6/group). (B) IVIS imaging of WT and *Nox1*$^{-/y}$*Nox4*$^{-/-}$ *mice* after L-012 injection (n = 5–6/group). (C) Ileal gene expression in WT and *Nox4*$^{-/-}$ mice (n = 9/group). (D) NOS2 immunoblots of ileal tissue derived from WT and *Nox4*$^{-/-}$ mice, tubulin as loading control. (E) Immunofluorescence of ileal tissue sections with NOX1 (red), NOS2 (green), and DAPI (blue); scale bar 100 μm. (F) L-012-mediated RONS detection in *Nox4*$^{fl/fl}$ *Vil*^{cre} mice, n = 5/group). (A, B, F) Two-way ANOVA with multiple comparisons test performed on normalized data; (C) *t*-test (*Nox1*, *Noxo1*), or Mann-Whitney test (*Nos2*).

and *Nox4*$^{-/-}$ mice indicated decreased Muc2-positive goblet cell numbers but similar mucus distribution, highlighting the flattened villus surface (Fig. S1B). The increase in Ki67 positive cells along the villi and in crypts in *Nox4*$^{-/-}$ mice suggests that the proliferation rate and the migration of epithelial cells is amplified (Fig. S1C). Expression analysis of selected cytokines and chemokines indicated upregulation of the IBD-associated markers *Il17a*, *Cxcl1* and *Cxcl2* (Fig. 1F). Overall, NOX4 deficiency led to spontaneous, age-dependent villus blunting, increased cytokine expression and epithelial disruption that is likely caused by oxidative damage.

NOX4 negatively regulates peroxynitrite formed by combined NOX1-NOS2 activity

L-012 mainly detects peroxynitrite ($ONOO^-$/ONOOH) and hypochlorous acid (HOCl) *in vivo* and does not react with hydrogen peroxide (H_2O_2)[2,26,27]. In unchallenged wildtype C57BL/6 mice, ileal peroxynitrite formation was entirely dependent on NOX1 and NOS2[25,28]. The highly increased ileal L-012 signal detected on *Nox4* deletion could either indicate considerable infiltration of activated neutrophils generating HOCl, or that H_2O_2 generation by constitutively active NOX4 suppresses in homeostasis the expression and/or activation of NOX1 or NOS2. Immune cell infiltration was not prominent (Fig. 1C), and thus we hypothesized that peroxynitrite levels were increased. The NOS inhibitors L-NAME or 1400 W were injected prior to L-012 IVIS imaging. Both inhibitors decreased the intestinal L-012 signal to baseline level (Fig. 2A, 1400 W not shown). To confirm the essential role of NOX1 in providing superoxide for $ONOO^-$/ONOOH generation, we crossed *Nox4*$^{-/-}$ mice with *Nox1*$^{-/y}$ mice. In *Nox1*$^{-/y}$*Nox4*$^{-/-}$ mice both the whole body and the intestinal L-012 signal were abolished (Fig. 2B), indicating that NOX4 activity restrains NOX1/NOS2-induced ileal peroxynitrite formation, preventing supra-physiological levels. Expression analysis by real time PCR and immunoblot were performed to assess how NOX4 exerts control over both enzymes. While *Nox1* showed only a trend towards transcriptional upregulation in the absence of NOX4, the expression of *Noxo1* (an essential NOX1 association partner) and *Nos2* were increased (Fig. 2C). Additionally, the expression of the H_2O_2 producing NADPH oxidase *Duox2* was increased (Fig. S2A), consistent with previous observations in dysbiosis, intestinal inflammation or microbial infection[2,6,16]. NOS2 protein was substantially upregulated in ileal tissue and on the tips of villi (Fig. 2D and E). While the NOX1 antibody was not sensitive enough to detect NOX1 in immunoblot, co-localization with NOS2 was observed in immunofluorescence of ileal tissue. It is important to consider that upregulation of *Nox1* is not required for increased NOX1 activity (ileal *Nox1* qPCR Ct24-25). Plasma membrane translocation, assembly and activation of the NOX1 complex by upstream signals will provide the defining input for catalytic activity.

Activated NOX1 is localized at the apical side of the ileal epithelium, mainly in enterocytes, but also in epithelial cycling cells and stem cells[29,30]. Reliable antibodies for detection of murine NOX4 are not available, confounding detailed localization analysis and our ability to determine whether cell intrinsic or cell extrinsic NOX4-dependent regulatory mechanisms contribute to changes in NOX1/NOS2 expression and catalytic activity. We generated *Nox4*$^{fl/fl}$ mice on a C57BL/6N background for Cre-mediated deletion of exons 7 and 8 (Fig. S2B) to analyze how tissue-specific deletion of *Nox4* alters ileal peroxynitrite generation. Global *Nox4* deletion, achieved after crossing *Nox4*$^{fl/fl}$ mice with CMV-cre deleter mice, recapitulated the changes observed in *Nox4*$^{-/-}$ mice (Figs. S1D and S2C). This result confirms independently the ileal phenotype of *Nox4*$^{-/-}$ mice generated by exon 4 replacement that were mainly used in this study. Subsequently, different compartments with reported *Nox4* expression were analyzed by using Vil-cre, LysM-cre and SMMHC-cre deleter mice to distinguish between intestinal epithelial cells, innate immune cells and stromal constituents as origin of NOX4 induced NOX1/NOS2 regulation. Whole body and *ex vivo* intestinal imaging with L-012 revealed that the increased ileal flux in *Nox4*$^{fl/fl}$*Vil*^{cre} mice resembled global *Nox4* deficient mice, while constitutive deletion of *Nox4* in innate immune cells or inducible deletion in smooth muscle cells showed no significant effect (Figs. 2F, S2D and E). The importance of NOX1 in mediating the increased ileal peroxynitrite generation observed in NOX4 deficient mice was further strengthened by crossing *Nox4*$^{-/-}$ mice to *Cybb*$^{-/y}$ mice (NOX2 deleted, no effect) or to *Cyba*^{nmf333} mice (NOX1-3 inactivated[2], signal abolished) (Fig. S2F). Thus, the H_2O_2 producing NADPH oxidase NOX4 negatively regulates ileal NOX1 function in mice.

Inflammation-associated ileal microbiome in Nox4$^{-/-}$ *mice*

Ileitis severity in mice is associated with compositional and functional dysbiosis of the intestinal commensal microbiota[31,32]. Modest differences in bacterial communities were reported in *Nox1*$^{-/y}$ mice in the small intestine, colon or in fecal pellets[28,33]. To understand the impact of peroxynitrite overproduction on bacterial and fungal communities, the ileal content of *Nox1*$^{-/y}$ mice was compared to *Nox4*$^{-/-}$ mice, *Nox1*$^{-/y}$*Nox4*$^{-/-}$ mice and their respective internal control wildtype mice. Substantial variability in microbial abundance in each group was observed, with the profile of ileal microbiota derived from NOX4-deficient mice showing more consistency and difference when compared to the other groups (Fig. 3A–C). The Inverse Simpson index of bacteria identified by shotgun metagenomics in the ileal content of *Nox4*$^{-/-}$ mice was significantly increased, while no differences in alpha diversity were observed between the other mouse strains (Fig. 3D). Compositional changes were only significant in *Nox4*$^{-/-}$ mice with decreased abundance of Actinobacteria, Bifidobacteria and Lactobacillus and an expansion of Bacteroidetes, especially of the family Muribaculaceae (formerly S24-7), suggesting inflammation-associated changes in the microbiome of NOX4 deficient mice (Fig. 3E and F). *Nox1*$^{-/y}$*Nox4*$^{-/-}$ mice displayed a mixed phenotype in alpha diversity and microbiota composition trending towards wildtype and NOX1 deficient mice. The ileal mycobiome is altered in CD patients, but analysis of the ileal murine mycobiome showed no significant differences in alpha/beta diversity or fungal abundance between any mouse strains except for significant *Aspergillus flavus* expansion in *Nox4*$^{-/-}$ mice (Fig. S3A–F).

Loss of ileal peroxynitrite correlates with disease progression in SAMP1/YitFc mice

SAMP1/YitFc mice represent a unique ileitis model that mimics many of the features of Crohn's disease. Pathogenesis is characterized by the spontaneous, progressive development of transmural ileitis leading to substantial hypertrophy of the muscularis propria (Fig. 4A[16]). To better understand the role of peroxynitrite in ileitis, expression of the NOX1 enzyme complex (*Nox1*, *Noxo1*, *Noxa1*) and *Nos2* in ileal tissue derived from 4-week, 16-week, and 40-week-old SAMP1/YitFc mice was determined. At 4 weeks, before onset of inflammation, expression of *Nox1* but not *Nos2* was moderately decreased in SAMP1 mice and control AKR mice (Fig. 4B). At the peak of inflammation (16 weeks) the NOX1 complex and *Nos2* were significantly downregulated in SAMP1/YitFc mice with expression levels not recovering as mice aged (40 weeks) (Figs. 4B and S4A). Accordingly, the nitrate levels were downregulated in the ileal tissue of SAMP1/YitFc mice and arginase 1, driving the arginine to ornithine pathway, was upregulated (Fig. S4B and C). As observed in *Nox1*$^{-/y}$[2,25] and *Nox4*$^{-/-}$ mice, downregulation of NADPH oxidase isoforms and the subsequent changes in host-microbiota interactions and/or intracellular signaling increased expression of *Duox2* (Fig. S4D). Considering that combined NOX1 and NOS2 activity is essential for ileal peroxynitrite generation, IVIS imaging using L-012 was performed on SAMP1/YitFc mice and AKR mice at different ages. The L-012 signal pattern differed between AKR and SAMP mice when analyzing intestinal compartments separately. No difference in whole body kinetics of mice at 16 weeks of age was observed, demonstrating

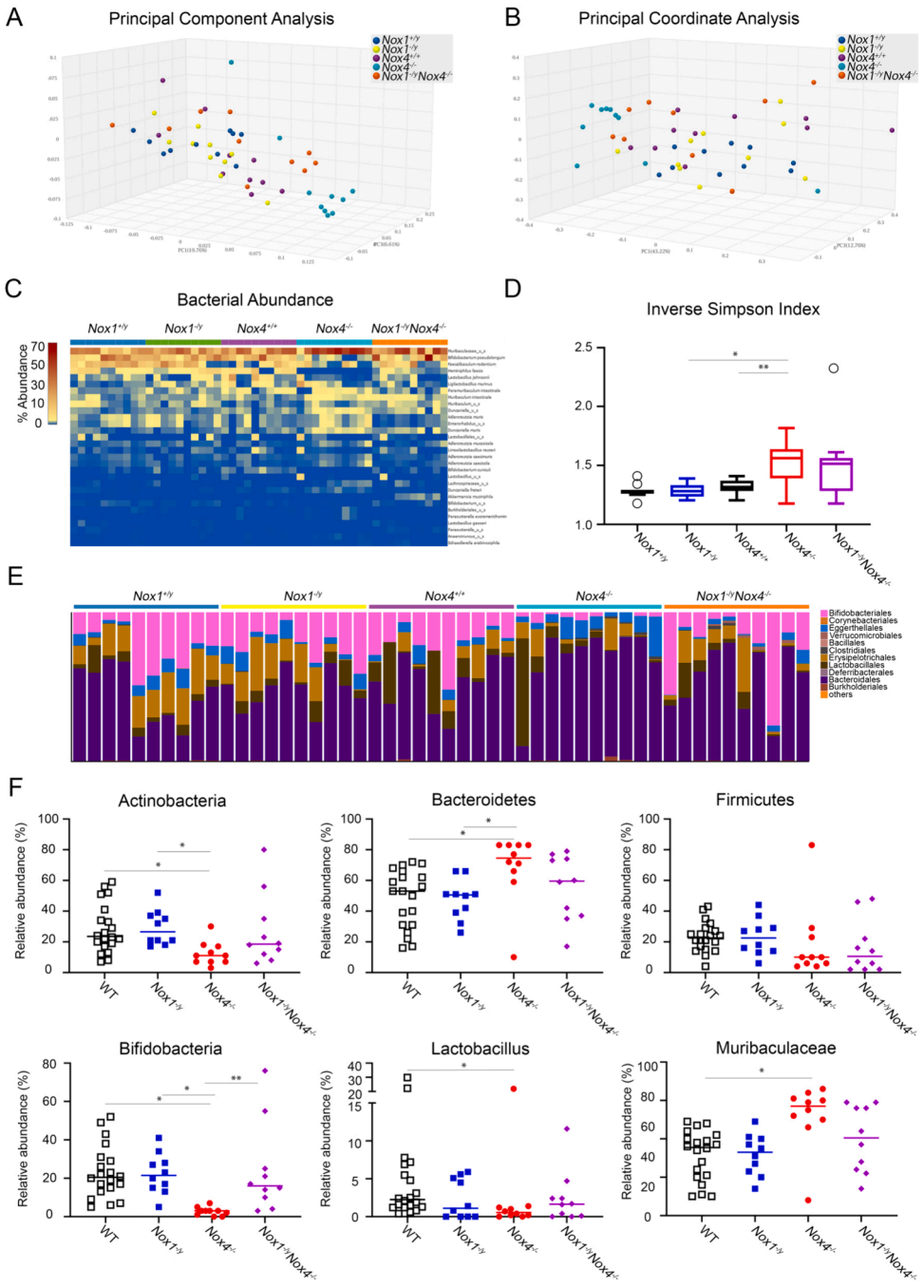

Fig. 3. Alterations of the ileal microbiome in *Nox4*$^{-/-}$ mice. Shallow shotgun sequencing and bioinformatic analysis of ileal contents derived from *Nox1*$^{+/y}$, *Nox1*$^{-/y}$, *Nox4*$^{+/+}$, *Nox4*$^{-/-}$ and *Nox1*$^{-/y}$ *Nox4*$^{-/-}$ mice (n = 10/group). (A) 3D Principal component analysis, (B) 3D Principal Coordinate Analysis, Plot of Bray-Curtis beta diversity. (C) Heat map of the 30 most abundant bacterial species, clustered by mouse genotype. (D) Inverse Simpson index. (E) Stacked bars depicting differences in order level bacteria. (F) Relative abundance of Actinobacteria, Bacteroidetes, Firmicutes, Bifidobacterium, Lactobacillus, and Muribaculaceae (WT combined to n = 20). One-Way ANOVA (Bacteroidetes, Bifidobacterium, Muribaculaceae) or Kruskal-Wallis test (Actinobacteria, Lactobacillus).

the importance of *ex vivo* analysis (Fig. 4C). Like C57BL/6 mice, AKR mice generated physiological levels of ileal peroxynitrite independently of age, while the L-012 signal intensity dropped significantly in the ileum of SAMP1/YitFc mice at 16 weeks and was even further reduced at 40 weeks, resembling background levels (Fig. 4C). Unexpectedly, a substantial L-012 signal was detected in the duodenum of SAMP1/YitFc mice at 16 weeks, which may indicate inflammation since duodenal *Nox1* and *Nos2* expression were enhanced (Fig. S4E). Inhibition of NOS2 activity decreased only partially the L-012 signal (Fig. S4F), indicating that peroxynitrite and another ROS, likely HOCl, were generated in the SAMP1/YitFc duodenum. SAMP1/YitFc mice develop immune-mediated gastritis with neutrophil accumulation, possibly leading to multiple proinflammatory changes in the duodenum[34]. Sequencing did not reveal any *Nox1* mutations in SAMP1/YitFc mice, indicating that downregulation of NOX1/NOS2 expression together with decreased catalytic activity of these enzymes, due to altered host-microbiome communication and dysbiosis, abolished ileal peroxynitrite generation in SAMP1/YitFc mice.

LPS cannot trigger ileal peroxynitrite generation in SAMP1/YitFc mice

We reported recently that NOX1 but not phagocyte NOX2 is essential

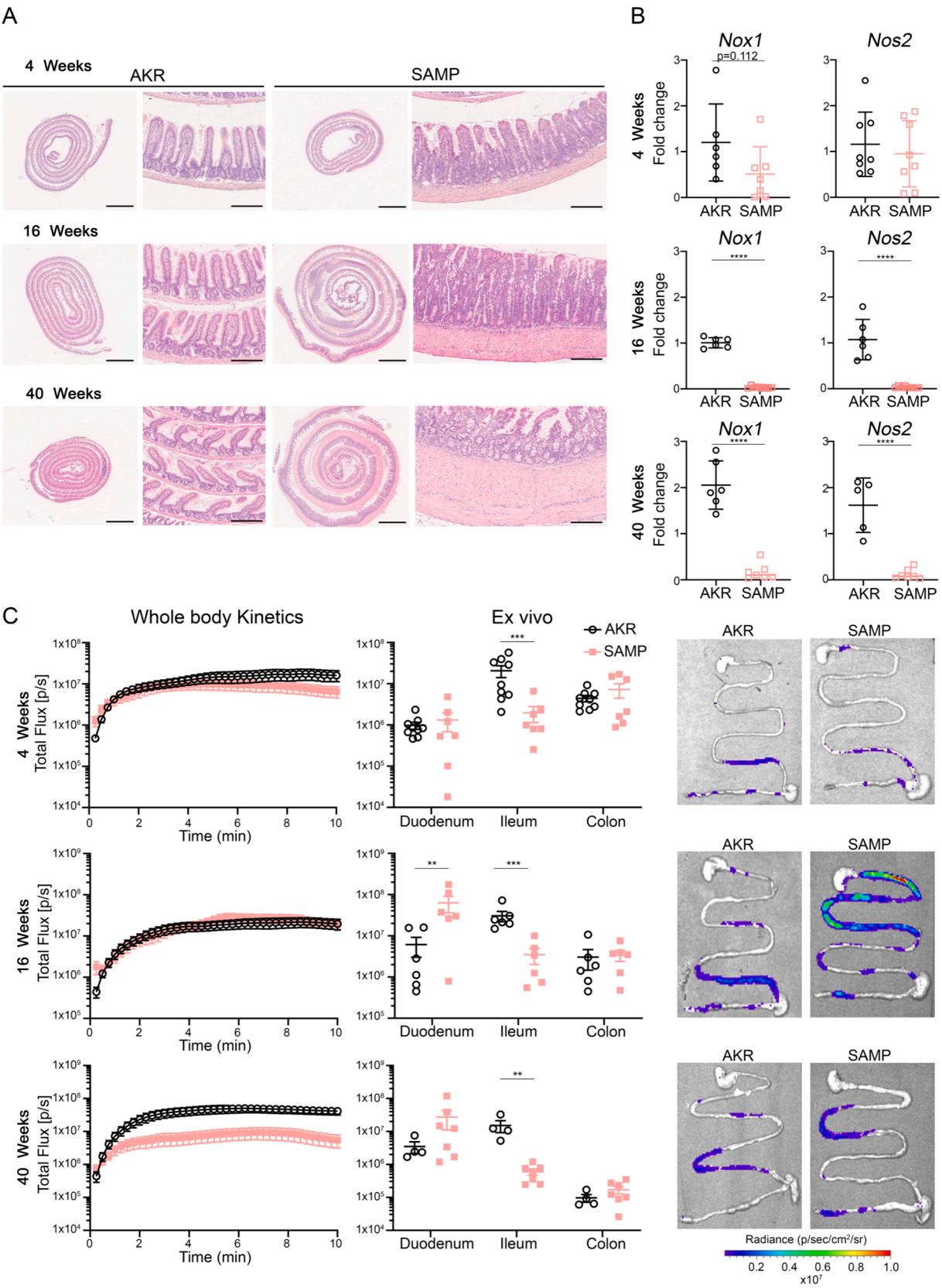

Fig. 4. Age-dependent histopathology in SAMP1/YitFc mice correlates with loss of ileal peroxynitrite generation and *Nox1/Nos2* expression. (A) H&E-stained intestine and ileal sections of AKR and SAMP1/YitFc mice aged 4, 16, and 40 weeks. Scale bars represent 2 mm and 200 μm. Transmural inflammatory cell infiltration (green arrow), and crypt hypertrophy with villous atrophy (yellow arrow) are shown. (B) Ileal expression of *Nox1* and *Nos2* in AKR and SAMP mice over time (n = 5–8/group) (C) 4-, 16- and 40-week-old SAMP1/YitFc (SAMP) and AKR/J (AKR) mice were injected with L-012 immediately before IVIS whole body and ex vivo imaging. 4 weeks (n = 7–9/group), 16 weeks (n = 6/group), 40 weeks (n = 4–7/group). T-test (B), two-way ANOVA with multiple comparisons performed on log-transformed data (C).

for LPS-mediated peroxynitrite generation in the intestine[25]. Earlier studies evaluated the effect of LPS stimulation on bone marrow-derived macrophages (BMDM) generated from SAMP1/YitFc mice and AKR mice, and reported comparable secretion of the cytokines TNFα, IL-6, and IL-1α[35]. The whole-body L-012 signal in 16-week-old female SAMP1/YitFc mice showed an initial decrease before recovering, suggesting delayed tissue distribution of L-012 in LPS conditions (Fig. 5A). As in C57BL/6 mice, the L-012 signal increased substantially in the ileum and colon of AKR mice after LPS exposure (Fig. 5B and C). Male and female SAMP1/YitFc mice responded to LPS by increasing L-012

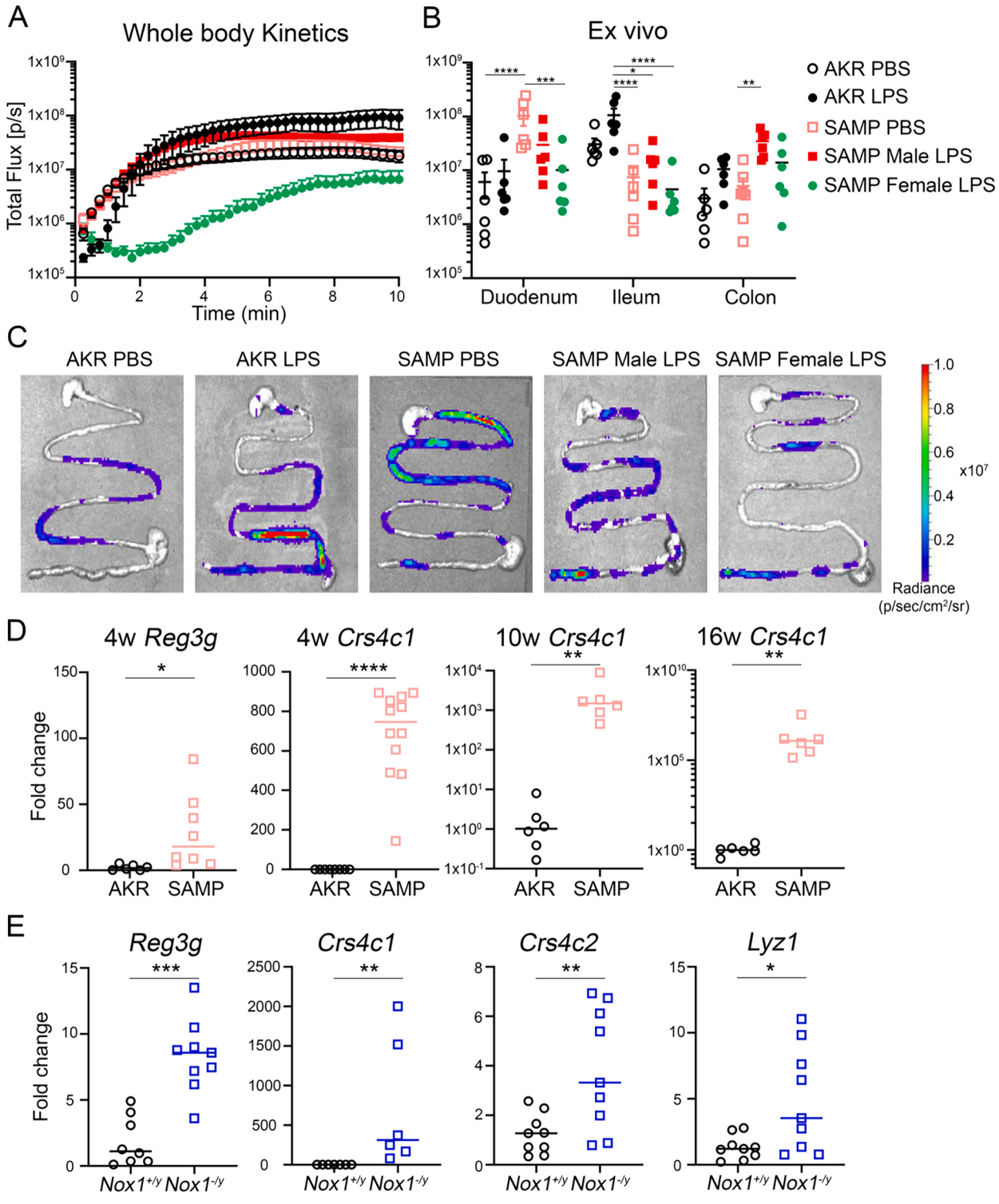

Fig. 5. NOX1 deficiency phenotype in SAMP1/YitFc mice. 16-week-old SAMP and AKR mice were injected with LPS or PBS 6 h prior to IVIS imaging (n = 5–6/group). (A) Kinetic curves, (B) *ex vivo* analyses, (C) and representative images of excised intestines are shown. (D) Ileal gene expression of antimicrobial peptides in AKR and SAMP mice at 4, 10 and 16 weeks (n = 6–12/group). (E) Ileal gene expression of antimicrobial peptides in *Nox1*$^{+/y}$ and *Nox1*$^{-/y}$ mice at 12 weeks (n = 6–9/group). (B) Two-way ANOVA with multiple comparisons was performed on log-transformed data. (D) T-test (*Reg3g*), Mann-Whitney test (*Crs4c1*); (E) T-test (*Lyz1*, *Crs4c1*, *Crs4c2*), Mann-Whitney test (*Reg3g*).

luminescence in the colon, but not in the ileum. In contrast, the distinct duodenal signal was reduced by LPS, showing less intensity and some patchiness. Thus, 16-week-old SAMP1/YitFc mice react to low-dose LPS by generating peroxynitrite in the colon, but not in the ileum. Ileal *Nox1* and particularly NOS2 expression levels were upregulated by exposure to LPS (Fig. S5A and B), suggesting that certain TLR4-mediated signals were not transmitted properly to assemble and activate the NOX1 complex.

Deficiency in NOX1 signaling amplifies generation of antimicrobial peptides

Paneth cell abnormalities are commonly observed in Crohn's disease pathophysiology and in murine ileitis models. Characterization of Paneth cells in SAMP1/YitFc mice showed an increased number of granules of non-uniform size, disordered endoplasmic reticulum (ER) structures and upregulation of ER stress markers, and changes in antimicrobial peptide (AMP) generation/folding[36,37]. Analysis of two representative AMPs indicated upregulation of *Reg3g* and age-dependent highly elevated *Crs4c1* generation in the ileal tissue of SAMP1/YitFc mice (Fig. 5D). As NOX1 function is compromised in the ileum of SAMP1/YitFc mice, we next assessed AMP expression in the terminal ileum of unchallenged *Nox1*$^{-/y}$ mice. The transcription of *Reg3g*, *Crs4c1*, *Crs4c2* and *Lyz1* was significantly increased (Fig. 5E), although inter-individual heterogeneity in AMP expression may indicate variation in the ileal microbiota composition. Abnormalities in Paneth cell location or abundance were not apparent in immunofluorescence staining of ileal tissue of *Nox1*$^{-/y}$, *Nox4*$^{-/-}$ or *Nox1*$^{-/y}$*Nox4*$^{-/-}$ mice (Fig. S5C). The amplified NOX1 activity in NOX4 deficient ileum did not alter *Crs4c1* transcription (Fig. S5D), suggesting that AMPs are upregulated when the NOX1-NOS2 axis fails.

Discussion

A limited number of spontaneous ileitis mouse models are currently available[38–40]. Only two of these models, the congenic SAMP1/YitFc strain and the transgenic TNF overexpressing *Tnf* $^{\Delta ARE}$ mice, reflect many characteristics of human CD. Early epithelial barrier dysfunction preceded the development of ileitis in SAMP1/YitFc mice and is part of the phenotype of *TNF* $^{\Delta ARE}$ pigs[40]. Changes in the intestinal stem cell niche, particularly Paneth cell alterations, were reported, accompanied by villus distortions, skip lesions, and granulomas, thereby mimicking CD ileitis. Microbiota is intimately involved in the ileitis phenotype as germ-free (GF) *Tnf* $^{\Delta ARE}$ mice remained disease-free, while GF SAMP1/YitFc mice displayed milder and delayed inflammation. We show here that NOX4 deficiency resulted in increased permeability, amplified peroxynitrite formation, augmented chemokine/cytokine production, villus blunting, and microbial dysbiosis. Mice with *Nox1* or combined *Nox4/Nox1* ablation did not exhibit an ileal phenotype, suggesting that ileal damage in *Nox4*$^{-/-}$ mice was triggered by excessive peroxynitrite generation. A highly oxidative environment can lead to ileocolitis over time as shown in mice deficient in glutathione peroxidases (*GPx1*$^{-/-}$*GPx2*$^{-/-}$). Crossing *GPx1*$^{-/-}$*GPx2*$^{-/-}$ mice with *Nox1*$^{-/y}$ mice attenuated the ileal GPx1/2 deficiency phenotype that included epithelial apoptosis, increase in Ki67 positive cells, and partial loss of Paneth cells[41]. Modification of the chemical environment i.e. changes in the RONS concentration alters host cell signaling and affects the microbiome. As observed in CD patients and other murine ileitis models, the ileal microbiota composition was altered in *Nox4*$^{-/-}$ mice with expansion of inflammation-associated Bacteroidetes, especially the family Muribaculaceae, and reduced abundance of *Bifidobacterium* and *Lactobacillus*. In contrast, ileitis prone *Ship*$^{-/-}$ mice showed reduced abundance of Muribaculaceae and expansion of *Lactobacillus*[42]. Recent evidence suggests that 'pathogenic' alteration of the intestinal microbiome occurs several years prior to onset of CD[43]. Granulomas or altered Paneth cell numbers, characteristic of CD-like ileitis, were not observed in NOX4 deficient ileum. In contrast to the dysbiosis observed in *Nox4*$^{-/-}$ mice, eliminating physiological peroxynitrite levels by *Nox1* ablation did not substantially modify the ileal microbiota. This suggests that damage to the ileal epithelium secondary to supra-physiological peroxynitrite levels may constitute a 'single hit' in the complex etiology of CD ileitis, mediated by microbiome modification.

At homeostasis, endogenous NOX4 maintains NOX1/NOS2-generated ileal peroxynitrite at physiological levels. Expression of transcriptionally regulated *Nox4* is stable in SAMP1/YitFc mice during the progression to inflammation and fibrosis[16], suggesting that this oxidase is not key in processes leading to progressive NOX1/NOS2 downregulation. While reliable antibodies for detecting murine NOX4 in distinct ileal cell types are not available, quantitative PCR of ileal tissue detected *Nox4* at Ct26-28 (AKR) and Ct25-27 (SAMP1/YitFc) at all ages. By screening tissue-specific *Nox4* deletion strains for peroxynitrite formation we identified villin expressing cells as potential origin of ileal NOX4 activity, albeit involvement of another cell type cannot be excluded. Single cell RNA-Seq of ileal CD tissues detected *NOX4* only in stroma (fibroblasts, smooth muscle cells)[29]. Stromal niche signals can affect intestinal stem cells and Paneth cells that express NOX1 and NOS2[44,45], implicating possibly long range signaling of NOX4-generated H_2O_2.

In acute LPS-induced sepsis, peroxynitrite formation in the murine intestine remains dependent on NOX1 and NOS2[25,28]. LPS-mediated signals for NOX1/NOS2 activation were preserved in the colon of older SAMP1/YitFc mice but abolished in the ileum. The ileum and colon differ substantially in terms of the chemical, physical and microbiological environment including oxygen concentration, mucus layer properties, and microbial density and composition. Differences in signaling are therefore expected and have been described for the NADPH oxidase DUOX2. Sommer *et al.* reported that microbiota-induced ileal *Duox2* expression was dependent on TRIF-mediated signaling to NF-κB, while a MyD88/p38 pathway was involved in colonic *Duox2* upregulation[46]. Others reported that increased NOX1 expression in LPS-stimulated colonic spheroids was MyD88-dependent[44], however ileal spheroids were not generated. Both NOX1 and NOS2 are expressed in the stem cell niche as well as in enterocytes[44,45]. Enteroids could not be established from *Nos2*$^{-/-}$ mice or inflamed SAMP/YitFc mice, while NOX1-deficient enteroids formed but proliferated less[45,47,48]. Downregulation of NOX1 and/or NOS2 signaling in older SAMP1/YitFc mice may contribute to their stem cell niche defects.

The antimicrobial defense system in the small intestine includes a single mucus layer and the regulated secretion of AMPs including α- and β-defensins, cathelicidins, lysozyme and others[49]. In mice, α-defensins are termed cryptdins and encompass 19 peptides and 6 cryptdin-related sequence (CRS) peptides, all secreted by Paneth cells. AMP production is dependent on the presence of microbiota, and vice versa changes in the abundance of certain AMPs shape the ileal microbiota composition. We propose that continuous generation of physiological levels of peroxynitrite constitutes an additional defense mechanism in the ileum, the area with the highest microbial load in the small intestine, by enforcing spatial segregation. Loss of this defense mechanism, as shown in NOX1 deficient and SAMP1/YitFc mice, results in compensation, at least in inbred mice in stable environmental conditions. In contrast to an earlier report[36], the AMP *Crs4c1* was progressively elevated in an age/disease-dependent manner in SAMP1/YitFc mice (Fig. 5D), with the unrelated C-type lectin *Reg3g* also being amplified. *Nox1*$^{-/y}$ mice cannot produce any peroxynitrite although, in contrast to SAMP1/YitFc mice, their nitric oxide production remains[25]. CRS4c peptides as well as *Reg3g* and *Lyz1* were upregulated in the ileum of *Nox1*$^{y/-}$ mice (Fig. 5E). Notably, ileal NOX1 and NOS2 expression and their activity are regulated by microbiota[25]. Taken together, these findings reinforce the notion of a collective system of oxidases, RONS and AMPs engaging bidirectionally with the ileal microbiota, where persistent changes in NADPH oxidase function may contribute to dysbiosis and inflammation.

Methods

Reagents

L-012 sodium salt (Fujifilm Wako), ProLong™ Glass Antifade Mountant with NucBlue™ Stain (Invitrogen), L-NG-Nitroarginine methyl ester (L-NAME), lipopolysaccharide *E. coli* O111:B4 (LPS) (all Sigma-Aldrich), FITC-dextran (TdB labs), 1400 W (MedChemExpress).

Mice

C57BL/6J (JAX000664), B6.129X1-*Nox1*^{tm1Kkr}/J (*Nox1*$^{-/y}$) (JAX018787), B6.129S-*Cybb*^{tm1Din}/J (*Cybb*$^{-/y}$) (JAX002365), A.B6 *Tyr* + -*Cyba*^{nmf333}/J (*Cyba*^{nmf333}) (JAX005445), B6.129-*Nox4*^{tm1Kkr}/J (*Nox4*$^{-/-}$) (JAX022996), SAMP1/YitFcsJ (SAMP) (JAX009355), AKR/J (AKR) (JAX000648), C57BL/6N-*Nox4*^{tm1820Arte} (*Nox4*$^{fl/fl}$) (this publication), B6.Cg-Tg(Vil1-cre)1000Gum/J (*Vil*^{cre}) (JAX021504), B6.129P2-*Lyz2*$^{tm1(cre)Ifo}$/J (*LysM*^{cre}) (JAX004781), B6.C-Tg(CMV-cre)1Cgn/J (*CMV*^{cre}) (JAX006054), B6.FVB-Tg(Myh11-icre/ERT2)1Soff/J (*SMA*^{cre}, SMMHC). Internal *Nox1*$^{+/y}$ and *Nox4*$^{+/+}$ control mice were generated by crossing *Nox1*$^{-/y}$ or *Nox4*$^{-/-}$ mice with C57BL/6J mice to the F3 generation. Other mice were crossed to create *Cybb*$^{-/y}$ *Nox4*$^{-/-}$, *Nox1*$^{-/y}$ *Nox4*$^{-/-}$, *Cyba*^{nmf333}*Nox4*$^{-/-}$, *Nox4*$^{fl/fl}$*CMV*^{cre}, *Nox4*$^{fl/fl}$*Vil*^{cre}, *Nox4*$^{fl/fl}$*LysM*^{cre}, *Nox4*$^{fl/fl}$*SMA*^{cre} mice strains. 11–12-week-old *Nox4*$^{fl/fl}$*SMA*^{cre} mice were injected i.p. with 100 µl of corn oil with and without tamoxifen (1 mg) on 5 consecutive days and used 3 weeks later. Female and male mice (4-, 12-, 16-, 40-weeks) were used. Analysis of NOX4 deficient mice was mainly performed in 16-week-old male mice as female mice showed delayed and varying development of the ileal phenotype. Mice were housed in IVC cages with enrichment in SPF conditions following FELASA guidelines. Mice received *ad libitum* purified water and irradiated chow (Teklad Global 18 % Protein diet, Envigo). Internal WT C57BL/6 mice were created, or AKR/J mice were used. established as crossing of C57BL/6 mice the appropriate knockout strains. Animal experiments followed the EU Directive 2010/63/EU and were approved by the UCD Animal Research Ethics Committee and the Health Products Regulatory Authority of Ireland.

IVIS imaging

Mice were anesthetized with 5 % isoflurane and injected i.p with L-012 (20 mg/kg) in H_2O directly before whole body imaging for 10 min, with 5sec or 2 min exposures using the IVIS® Spectrum CT (Perkin Elmer). Immediately after euthanasia the intestines were excised and imaged for a further 5sec exposure. Total flux of the abdomen or GI tract areas was calculated as photons/sec. LPS (2.5 mg/kg), L-NAME (50 mg/kg), 1400 W (20 mg/kg), or PBS control were i.p. injected 6 h before imaging.

Intestinal function

The integrity of the intestinal epithelial barrier was determined by oral gavage of 80 mg/ml 4 kDa FITC-dextran (150 µl/mouse; 6wk/16wk-old mice). 4 h later blood was collected, and permeability was analyzed as described[2]. Intestinal motility in 8-week-old mice was assessed by oral gavage with 200 µl of a charcoal solution (4 % charcoal in 2 % carboxymethyl cellulose). 20 min later the small intestine was collected from euthanized animals, and the distance travelled by the charcoal from pylorus to cecum was measured by a ruler and expressed as percentage of the total distance.

Histology and immunofluorescence

Paraffin-embedded ileal samples fixed in 10 % neutral-buffered formalin (in methanol-Carnoy's solution for Mucin2 staining) were sectioned, de-paraffinized, rehydrated, and stained with H&E progressive protocol (using Mayer's Hematoxylin, counterstained with Eosin-Y). Slides were mounted with DPX New Mounting Solution (Merck), and digitally scanned with an Aperio ScanScope XT scanner. De-paraffinized tissue sections were also subjected to antigen retrieval using 10 mM sodium citrate (pH 6.0), followed by blocking in 5 % goat serum/1% BSA/0.1 % Triton-X100 in PBS, and probed with APC conjugated anti-NOS2 antibody (17–5920-80, Invitrogen), anti-NOX1 antibody (rat anti-mouse[30,50]), anti-lysozyme antibody (611375, Cell Signaling), anti-Mucin2 (H-300) antibody (sc-15334, Santa Cruz), or anti-Ki67 (SP6) antibody (ab16667, Abcam), followed by Alexa Fluor coupled secondary antibodies (Invitrogen). Images were acquired with an Olympus FV3000 confocal microscope or an LSM 800 Airyscan (Zeiss) using a 20X air objective and processed using ICY imaging software.

Scanning electron microscopy (SEM)

Ileal segments were harvested from euthanized mice, opened laterally, and fixed in 2.5 % glutaraldehyde and 2.5 % paraformaldehyde in 0.1 M Sørensen's phosphate buffer. Fixed samples were washed twice with Sørensen's phosphate buffer, post fixed in 1 % osmium tetroxide and washed twice with Sørensen's phosphate buffer. Subsequently, the specimens were dehydrated in a graded ethanol series and hexamethyldisilazane (HMDS). After air drying, samples were mounted on aluminum stubs, sputter-coated with a layer of gold and imaged with a Hitachi S-4300 at an accelerating voltage of 5 kV.

Tissue nitrate measurement

The modified Griess reaction was used to determine the nitrate concentration in tissues. 600 mg of terminal ileum tissue (~2cm) was collected, rinsed, and placed in 800 µl PBS with 0.5 g of 1 mm zircon beads in a 2 ml tube. Next, the samples were homogenized (MP Biomedicals homogenizer) at 4 ms-1 for two cycles of 60 s, with 120 s pause between cycles, and centrifuged at 20,000g for 20 min 4 °C. The standard curve ranged from 0.78-50 µM sodium nitrate, 100 µl of each concentration was added in duplicate to a clear 96-well plate. 100 µl of each supernatant sample was added to the plate (4x/assay), followed by 200 µl of Griess solution. Absorbance at 520 nm was read after 10 min and 4 h incubation at 37 °C in the dark. For nitrate, the OD reading after 4 h was subtracted from the 10 min reading and interpolated to the nitrate standard curve.

Microbiome and mycobiome analysis

The luminal and loosely bound mucosa-associated content of the ileum (last quarter of the small intestine) of male mice (16-week-old, F3/F4 generation separated after F2, internal WT and knockout mice as indicated, no co-housing of different genotypes after F2) was collected. gDNA was extracted by mechanical homogenization using Lysing Matrix E tubes (MP Biomedicals) combined with phenol chloroform extraction. Briefly, 500 µl of extraction buffer (2 %Triton X-100, 100 mM NaCl, 10 mM Tris pH7.4, 1 mM EDTA, 1 %SDS in dH_2O) and 500 µl of phenol: chloroform: isoamyl alcohol mixture was added to 2 ml Lysing Matrix E tubes (1.4 mm ceramic sphere, 0.1 mm silica spheres, one 4 mm glass bead, MP biomedical) containing luminal content. After homogenization (5x30sec, 5 ms^{-1}) the upper aqueous layer was collected; this process was repeated and gDNA was precipitated with ethanol and 7.5 M ammonium acetate (Sigma-Aldrich), resuspended in TE buffer (Qiagen) and quantified. Shallow shotgun sequencing (3 M Read, 0.5 Gb) for bacteria and ITS 1&2 amplicon sequencing for fungi was performed by CosmosID (Germantown, USA). The prepared libraries were sequenced on an Illumina NextSeq 2000 platform (2x150 for bacteria, 2x250 for fungi). Raw reads from paired-end or single-end Fastq files were trimmed to remove adapters and bases of low quality. Fungi bioinformatic analysis involved OTUs being identified against the UNITE fungal

database using a closed-reference OTU picker and 97 % sequence similarity through the QIIME framework. For bacteria, the pipeline had two separable comparators: initially a pre-computation phase for reference databases followed by a second per-sample computation. The input to the pre-computation phase were databases of reference genomes curated by CosmosID. Taxonomic profiling and data visualization were automatically provided in the CosmosID-HUB (CosmosID Metagenomics Cloud, app.cosmosid.com, CosmosID Inc.).

Real-time PCR

RNA was isolated from the terminal ileum using the RNeasy Mini Kit (Qiagen) and reverse transcribed using the High-Capacity cDNA Reverse Transcription kit (Thermo Fisher Scientific). qPCR was performed with a 7500 Fast Real Time PCR System using the Taqman® Fast Universal PCR Master Mix and Taqman Gene Expression Assays (Applied Biosystems). Gene expression levels were normalized to *Gapdh*, and data were analyzed by $2-\Delta\Delta$Ct or by inverse delta Ct. Taqman probes used: *Arg1*-*Mm00475988_m1*, *Ccl2*-Mm00441242_m1, *Crs4c1*-Mm00655851_gH, *Crs4c2*-Mm04205949_gH, *Cxcl1*-Mm04207460_m1, *Cxcl2*-Mm00436450_m1, *Duox2*-Mm01326247_m1, *Lyz1*-m00657323_m1, *Il17a*-Mm00439618_m1, *Nos2*-Mm00440485_m1, *Nox1*-Mm00549170_m1, *Noxo1*-Mm04209048_g1, *Noxa1*-Mm00549172_m1, *Reg3g*-Mm01181783_g1, *Gapdh*-Mm99999915_g1 (Applied Biosystems).

Immunoblotting

For mucosal scrapings: The distal 2 cm of the ileum were opened longitudinally, cleaned of content using the straight edge of a spatula, then immersed in 30 mM EDTA for 5 min. The tissue was then blotted dry and placed mucosal side upwards on a plastic surface. The mucosa was gently scraped off using the straight edge of a spatula, placed in a tube and snap frozen. Protein was extracted using RIPA buffer and membranes were probed with antibodies directed to NOS2 (610329, BD Biosciences), α-tubulin (T6199, Sigma Aldrich), and β-tubulin (ONS.1A6, Sigma-Aldrich). The secondary antibodies were HRP-conjugated goat anti-mouse antibodies (Southern Biotech). Protein bands were detected using ECL (Pierce).

Statistical analysis

For statistical analysis, unpaired Student's *t*-test (two-tailed) or a 2-way ANOVA with multiple comparisons was performed on normal distributed data. Multiple comparisons were corrected by using the Tukey *post-hoc* test. In some experiments the Mann-Whitney test or Kruskal-Wallis test were performed as indicated. All data were expressed as mean ± SD, except for IVIS experiments as mean ± SEM. All statistical analysis were performed using GraphPad Prism (version 8.4.3; GraphPad, San Diego). Each data point in figures represents 1 mouse, total n numbers of 2–3 repeats are indicated. Significance: ns, non-significant, *$P \leq 0.05$, **$P \leq 0.01$, ***$P \leq 0.005$), ****$P \leq 0.0001$.

Data availability

The datasets generated and analyzed for the current study have been uploaded to the NCBI SRA at //https://www.ncbi.nlm.nih.gov/sra under PRJNA1157016 and PRJNA1157020. Reagents and other data sets will be supplied on reasonable request.

Author contributions

UGK developed the concept and designed the study together with JW, JDLR, ES, YY, RJ, and GA. JDLR, JW, ES, YY, RJ, and GA performed experiments and data analysis. MM provided reagents. UGK wrote the manuscript with input of all authors.

CRediT authorship contribution statement

Julie Drieu La Rochelle: Writing – review & editing, Formal analysis, Data curation. **Josie Ward:** Writing – review & editing, Methodology, Formal analysis, Data curation. **Emily Stenke:** Writing – review & editing, Methodology, Funding acquisition, Formal analysis, Data curation. **Yuting Yin:** Writing – review & editing, Formal analysis, Data curation. **Misaki Matsumoto:** Writing – review & editing, Resources. **Richard Jennings:** Writing – review & editing, Methodology, Formal analysis, Data curation. **Gabriella Aviello:** Writing – review & editing, Investigation, Funding acquisition, Formal analysis, Data curation. **Ulla G. Knaus:** Writing – original draft, Writing – review & editing, Validation, Supervision, Resources, Project administration, Investigation, Funding acquisition, Conceptualization.

Declaration of Competing Interest

The authors declare that they have no known competing financial interests or personal relationships that could have appeared to influence the work reported in this paper.

Acknowledgements

We would like to thank the staff of the Biomedical Facility, Tiina O'Neill, Biological Imaging Facility, and Suisheng Zhang for support. This study was supported by the National Children's Research Centre (K-17-2, UGK), Science Foundation Ireland (16-IA-4501, 22/FFP-A/10349, UGK), the Health Research Board (2016-1677, ES), and NRRP project MNESYS (PE0000006), a multiscale integrated approach to the study of the nervous system in health and disease (DN.1553 11.10.2022, GA).

Appendix A. Supplementary data

Supplementary data to this article can be found online at https://doi.org/10.1016/j.mucimm.2024.08.012.

References

1. Birchenough GM, Nystrom EE, Johansson ME, Hansson GC. A sentinel goblet cell guards the colonic crypt by triggering Nlrp6-dependent Muc2 secretion. *Science*. 2016;352(6293):1535–1542.
2. Aviello G, Singh AK, O'Neill S, et al. Colitis susceptibility in mice with reactive oxygen species deficiency is mediated by mucus barrier and immune defense defects. *Mucosal Immunol*. 2019;12(6):1316–1326.
3. Aviello G, Knaus UG. NADPH oxidases and ROS signaling in the gastrointestinal tract. *Mucosal Immunol*. 2018;11(4):1011–1023.
4. Kunst C, Schmid S, Michalski M, et al. The influence of gut microbiota on oxidative stress and the immune system. *Biomedicines*. 2023;11(5).
5. Alvarez LA, Kovacic L, Rodriguez J, et al. NADPH oxidase-derived H2O2 subverts pathogen signaling by oxidative phosphotyrosine conversion to PB-DOPA. *Proc Natl Acad Sci USA*. 2016;113(37):10406–10411.
6. Pircalabioru G, Aviello G, Kubica M, et al. Defensive mutualism rescues NADPH oxidase inactivation in gut infection. *Cell Host Microbe*. 2016;19(5):651–663.
7. Hayes P, Dhillon S, O'Neill K, et al. Defects in NADPH oxidase genes NOX1 and DUOX2 in very early onset inflammatory bowel disease. *Cell Mol Gastroenterol Hepatol*. 2015;1(5):489–502.
8. Schwerd T, Bryant RV, Pandey S, et al. NOX1 loss-of-function genetic variants in patients with inflammatory bowel disease. *Mucosal Immunol*. 2018;11(2):562–574.
9. Parlato M, Charbit-Henrion F, Hayes P, et al. First identification of biallelic inherited DUOX2 inactivating mutations as a cause of very early onset inflammatory bowel disease. *Gastroenterology*. 2017;153(2):609–611 e603.
10. Falcone EL, Holland SM. Gastrointestinal complications in chronic granulomatous disease. *Methods Mol Biol*. 2019;1982:573–586.
11. Huang C, De Ravin SS, Paul AR, et al. Genetic risk for inflammatory bowel disease is a determinant of Crohn's disease development in chronic granulomatous disease. *Inflamm Bowel Dis*. 2016;22(12):2794–2801.
12. Dang PM, Rolas L, El-Benna J. The dual role of reactive oxygen species-generating nicotinamide adenine dinucleotide phosphate oxidases in gastrointestinal inflammation and therapeutic perspectives. *Antioxid Redox Signal*. 2020;33(5):354–373.
13. Bourgonje AR, Feelisch M, Faber KN, Pasch A, Dijkstra G, van Goor H. Oxidative stress and redox-modulating therapeutics in inflammatory bowel disease. *Trends Mol Med*. 2020;26(11):1034–1046.

14. Rhen M. Salmonella and reactive oxygen species: a love-hate relationship. *J Innate Immun*. 2019;11(3):216–226.
15. Marild K, Soderling J, Axelrad J, Halfvarson J, Forss A, Group SS, et al. Histologic activity in inflammatory bowel disease and risk of serious infections: a nationwide study. *Clin Gastroenterol Hepatol*. 2024;22(4):831–846.
16. Stenke E, Aviello G, Singh A, et al. NADPH oxidase 4 is protective and not fibrogenic in intestinal inflammation. *Redox Biol*. 2020;37, 101752.
17. Lee Y, Kim SH, Jeong H, et al. Role of Nox4 in mitigating inflammation and fibrosis in dextran sulfate sodium-induced colitis. *Cell Mol Gastroenterol Hepatol*. 2023;16(3):411–429.
18. Schroder K, Zhang M, Benkhoff S, et al. Nox4 is a protective reactive oxygen species generating vascular NADPH oxidase. *Circ Res*. 2012;110(9):1217–1225.
19. Gray SP, Di Marco E, Kennedy K, et al. Reactive oxygen species can provide atheroprotection via NOX4-dependent inhibition of inflammation and vascular remodeling. *Arterioscler Thromb Vasc Biol*. 2016;36(2):295–307.
20. Hahner F, Moll F, Warwick T, et al. Nox4 promotes endothelial differentiation through chromatin remodeling. *Redox Biol*. 2022;55, 102381.
21. Brewer AC, Murray TV, Arno M, et al. Nox4 regulates Nrf2 and glutathione redox in cardiomyocytes in vivo. *Free Radic Biol Med*. 2011;51(1):205–215.
22. Mir S, Golden BDO, Griess BJ, et al. Upregulation of Nox4 induces a pro-survival Nrf2 response in cancer-associated fibroblasts that promotes tumorigenesis and metastasis, in part via Birc5 induction. *Breast Cancer Res*. 2022;24(1):48.
23. Penuelas-Haro I, Espinosa-Sotelo R, Crosas-Molist E, et al. The NADPH oxidase NOX4 regulates redox and metabolic homeostasis preventing HCC progression. *Hepatology*. 2023;78(2):416–433.
24. Helfinger V, Freiherr von Gall F, Henke N, et al. Genetic deletion of Nox4 enhances cancerogen-induced formation of solid tumors. *Proc Natl Acad Sci U S A*. 2021;118(11).
25. Ward J, Zhang S, Sikora A, et al. VEO-IBD NOX1 variant highlights a structural region essential for NOX/DUOX catalytic activity. *Redox Biol*. 2023;67, 102905.
26. Asghar MN, Emani R, Alam C, et al. In vivo imaging of reactive oxygen and nitrogen species in murine colitis. *Inflamm Bowel Dis*. 2014;20(8):1435–1447.
27. Han W, Li H, Segal BH, Blackwell TS. Bioluminescence imaging of NADPH oxidase activity in different animal models. *J Visual Exper: JoVE*. 2012;68.
28. Matziouridou C, Rocha SDC, Haabeth OA, Rudi K, Carlsen H, Kielland A. iNOS- and NOX1-dependent ROS production maintains bacterial homeostasis in the ileum of mice. *Mucosal Immunol*. 2018;11(3):774–784.
29. Kong L, Pokatayev V, Lefkovith A, et al. The landscape of immune dysregulation in Crohn's disease revealed through single-cell transcriptomic profiling in the ileum and colon. *Immunity*. 2023;56(2):444–458 e445.
30. Liu J, Iwata K, Zhu K, et al. NOX1/NADPH oxidase in bone marrow-derived cells modulates intestinal barrier function. *Free Radic Biol Med*. 2020;147:90–101.
31. Schaubeck M, Clavel T, Calasan J, et al. Dysbiotic gut microbiota causes transmissible Crohn's disease-like ileitis independent of failure in antimicrobial defence. *Gut*. 2016;65(2):225–237.
32. Corridoni D, Rodriguez-Palacios A, Di Stefano G, et al. Genetic deletion of the bacterial sensor NOD2 improves murine Crohn's disease-like ileitis independent of functional dysbiosis. *Mucosal Immunol*. 2017;10(4):971–982.
33. Herfindal AM, Rocha SDC, Papoutsis D, Bohn SK, Carlsen H. The ROS-generating enzyme NADPH oxidase 1 modulates the colonic microbiota but offers minor protection against dextran sulfate sodium-induced low-grade colon inflammation in mice. *Free Radic Biol Med*. 2022;188:298–311.
34. Reuter BK, Pastorelli L, Brogi M, et al. Spontaneous, immune-mediated gastric inflammation in SAMP1/YitFc mice, a model of Crohn's-like gastritis. *Gastroenterology*. 2011;141(5):1709–1719.
35. Corridoni D, Kodani T, Rodriguez-Palacios A, et al. Dysregulated NOD2 predisposes SAMP1/YitFc mice to chronic intestinal inflammation. *Proc Natl Acad Sci USA*. 2013;110(42):16999–17004.
36. Shanahan MT, Vidrich A, Shirafuji Y, et al. Elevated expression of Paneth cell CRS4C in ileitis-prone SAMP1/YitFc mice: regional distribution, subcellular localization, and mechanism of action. *J Biol Chem*. 2010;285(10):7493–7504.
37. Shimizu Y, Nakamura K, Yoshii A, et al. Paneth cell alpha-defensin misfolding correlates with dysbiosis and ileitis in Crohn's disease model mice. *Life Sci Alliance*. 2020;3(6).
38. Iliopoulou L, Kollias G. Harnessing murine models of Crohn's disease ileitis to advance concepts of pathophysiology and treatment. *Mucosal Immunol*. 2022;15(1):10–26.
39. Cominelli F, Arseneau KO, Rodriguez-Palacios A, Pizarro TT. Uncovering pathogenic mechanisms of inflammatory bowel disease using mouse models of Crohn's disease-like ileitis: what is the right model? *Cell Mol Gastroenterol Hepatol*. 2017;4(1):19–32.
40. Metwaly A, Haller D. The TNFΔARE model of Crohn's disease-like Ileitis. *Inflamm Bowel Dis*. 2024;30(1):132–145.
41. Esworthy RS, Kim BW, Chow J, Shen B, Doroshow JH, Chu FF. Nox1 causes ileocolitis in mice deficient in glutathione peroxidase-1 and -2. *Free Radic Biol Med*. 2014;68:315–325.
42. Dobranowski PA, Tang C, Sauve JP, Menzies SC, Sly LM. Compositional changes to the ileal microbiome precede the onset of spontaneous ileitis in SHIP deficient mice. *Gut Microbes*. 2019;10(5):578–598.
43. Raygoza Garay JA, Turpin W, Lee SH, et al. Gut microbiome composition is associated with future onset of Crohn's disease in healthy first-degree relatives. *Gastroenterology*. 2023;165(3):670–681.
44. van der Post S, Birchenough GMH, Held JM. NOX1-dependent redox signaling potentiates colonic stem cell proliferation to adapt to the intestinal microbiota by linking EGFR and TLR activation. *Cell Rep*. 2021;35(1), 108949.
45. Huang L, Xu Z, Lei X, et al. Paneth cell-derived iNOS is required to maintain homeostasis in the intestinal stem cell niche. *J Transl Med*. 2023;21(1):852.
46. Sommer F, Backhed F. The gut microbiota engages different signaling pathways to induce Duox2 expression in the ileum and colon epithelium. *Mucosal Immunol*. 2015;8(2):372–379.
47. Butto LF, Pelletier A, More SK, et al. Intestinal stem cell niche defects result in impaired 3D organoid formation in mouse models of Crohn's disease-like ileitis. *Stem Cell Rep*. 2020;15(2):389–407.
48. Lee C, Hong SN, Kim ER, Chang DK, Kim YH. Depletion of intestinal stem cell niche factors contributes to the alteration of epithelial differentiation in SAMP1/YitFcsJ mice with Crohn disease-like ileitis. *Inflamm Bowel Dis*. 2021;27(5):667–676.
49. Muniz LR, Knosp C, Yeretssian G. Intestinal antimicrobial peptides during homeostasis, infection, and disease. *Front Immunol*. 2012;3:310.
50. Diebold BA, Wilder SG, De Deken X, et al. Guidelines for the detection of NADPH oxidases by immunoblot and RT-qPCR. *Methods Mol Biol*. 2019;1982:191–229.